On Stall Behavior in Aerobatic Figures with an Aerobatic Glider

Regine Pattermann, Fabian Sturm and Benedikt Döller
r.pattermann@akaflieg-muenchen.de
Akaflieg München e.V.
Technische Universität München
Munich, Germany

Abstract

In order to optimize stall behavior of aerobatic gliders in aerobatic figures, which include rapid autorotational spins like snap rolls, research on aerodynamics that leads to the necessary stall is needed. Combined trailing- and leading-edge stall is found to be the most convenient stall type to be aimed for in an aerobatic glider. Investigations using XFOIL, as well as CFX, a numerical CFD method by ANSYS, wind tunnel experiments and flight tests are carried out to learn more about flow separation at the leading edge. The focus of this work is the laminar separation bubble that forms at the leading edge of the wing. There exist different ideas of predicting its behavior around the maximum lift-coefficient and the resulting type of stall. Ultimately, this paper examines what happens during flow separation at the leading edge of existing aerobatic gliders and the newly designed Mue 13-33 airfoil. It was found, that the laminar separation bubble, which forms at the leading edge at high angles of attack, remains there during and after stall and therefore has no direct influence on the stall process. This stall behavior is not described in existing literature so far.

Introduction

Akaflieg München is currently developing an aerobatic glider called the Mü 32 Reißmeister with the intent of incorporating all positive characteristics of existing designs. These characteristics are agility, high roll rate, identical properties in normal and inverted flight and stall characteristics suitable for aerobatic figures, including autorotational maneuvers such as snap rolls. To achieve these requirements, the development focuses on research and design of a symmetrical airfoil with an automatically controlled flap.

The snap roll turned out to present the main challenge of the airfoil design. To initiate the maneuver, a rapid stall is necessary, typically a leading edge stall on one entire wing. However, safe low-speed flying qualities need to be maintained, especially during take-off and landing. To achieve this, the solution is a combined trailing and leading edge stall. The pilot senses vibration in the stick due to the shed vortices hitting the elevator and can thus prevent the rapid occurrence of a leading edge stall with appropriate corrective control. Leading edge stall is intended to start following a further increase in angle of attack following the onset of trailing edge stall. By comparing two gliders from Margański and Mysłowski Aviation Works, the Swift S1 has these required stall characteristics. The MDM-1 Fox, however, while featuring the same wing airfoil as the Swift S1, has a less balanced overall concept in terms of stall behavior. This especially affects the flow reattachment process. Inertia effects due to mass distribution and wing geometry that may have a positive effect on different aerodynamic figures are responsible for a more difficult handling of MDM-1 Fox when stopping snap rolls.

This paper details a scenario that leads to rapid leading edge stall. The goals of the research presented below are the clarification of stall characteristics of the airfoils of the aerobatic gliders Swift S1 and MDM-1 Fox and, further, the development of the modern airfoil Mue 13-33 with similar stall behavior. The use of the term "leading edge stall" in this paper always refers to the stall that starts after the beginning of the trailing edge stall. Distinctions between different types of leading edge stall are made based on the presence of

(i) laminar flow separation or

(ii) involvement of a bubble or vortex at the leading edge.

Schlichting and Truckenbrodt [1] sum up observations on leading edge stall without bubble burst. Though a high angle of attack creates a laminar separation bubble at the leading edge, its size decreases with a further increase in angle of attack until it vanishes completely. After this, leading edge stall occurs due to the fact that the laminar flow is no longer able to follow the curvature of the airfoil. Transition does not appear close enough to the surface, so a laminar separation bubble does not form. Experimental and numerical research on stall behavior, including bubble burst, is typically performed on flat plates rather than wing airfoils. Growth of bubbles close to the maximum lift coefficient is characteristic of stalls that include a bubble burst. This

paper concentrates on transition, which influences the length and height of the bubble. Successful numerical simulation can only be performed for the transition process and growth of the laminar separation bubble, not on bubble burst [2]. Experimental research with a focus on bubble burst, as it can be found on thin airfoils, is presented by M. Gaster [3]. It is of a different character than stall on airfoils similar to Mue 13-33 and therefore beyond the scope of this research. See literature by several members of IAG Stuttgart [4], [5] and Diwan [6] for more information.

In the literature, the expression "bubble burst" is also used to describe the phenomenon of dynamic stall as it occurs on helicopter blades. One example of this use of expression is Greenblatt [7]. This process, however is highly unsteady and not comparable with the possible bubble burst that occurs in laminar separation bubbles. Dynamic stall caused by a vortex at the leading edge (referred to as bubble in older publications) can only be found on continuously oscillating wing sections and not due to one single increase in angle of attack. The main difference between bursts of laminar separation bubbles and dynamic stall is the following: the dynamic stall vortex develops within the first period of an oscillation and does not suddenly appear and burst following a rapid movement out of stationary flight [8]. The laminar separation bubble appears in steady flight and might burst due to a single event that leads to a change in flow.

Experimental and Numerical Work

Two different airfoils with similar properties are the focus of interest: the newly developed Mue 13-33 and the NACA 64_1-412 as wing section of the Swift S1 and the MDM-1 Fox. Numerical investigations and polar curves at steady wind tunnel conditions exist for both airfoils. In addition, there are oil-flow patterns and pressure distributions for the Mue 13-33. Flight tests with the Swift S1 and the MDM-1 Fox offer flow visualization by the use of oil flow patterns and tuft patterns.

In polar curves, the stall characteristic is partly visible as a rapid loss of lift coefficient with an increase in angle of attack by one degree only. Comparing steady wind tunnel measurements of the Mue 13-33 with steady flight test results of the NACA 64_1-412, combined with the knowledge of polar curves, allows an assessment of their relative suitability for snap rolls, even if experimental work at unsteady conditions for the Mue 13-33 is missing. The comparison also provides overall design guidance for the Mü 32 Reißmeister. In addition to the difficulties in comparing steady and unsteady increase in angle of attack, there is also the matter of two-dimensional wing sections vs. three-dimensional wings during stall. Three-dimensional effects on the two-dimensional wing section in the wind tunnel are visible in oil flow patterns and the experimental data can be judged with the aid of flight test observations. Nevertheless, three-dimensional effects should not be neglected when comparing polar curves derived from wind tunnel measurements.

For the development of the Mue 13-33 airfoil two different kinds of software are used. The first, XFOIL, is used for inverse

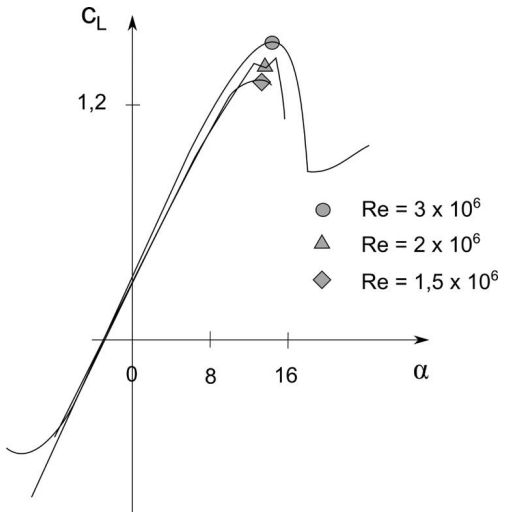

Fig. 1: Lift characteristics of NACA 64_1-412 airfoil at different Reynolds numbers [13].

airfoil design. It allows very good predictions when transition occurs while the boundary layer is attached, as well as prediction of lift and drag of the airfoil. Nevertheless, it cannot provide information on stall behavior [9]. The second software is ANSYS CFX, which is known to give reliable predictions on stall characteristics in various fluid dynamical considerations. A laminar separation bubble is expected to be involved in the stall, which leaves the γ-Re_θ-transition model, in combination with the SST-turbulence model, as a choice of numerical approach. No direct numerical simulation, other than Reynolds-averaged Navier-Stokes modeling, is used [9], [10].

Wind tunnel measurements were performed at the laminar wind tunnel at IAG Stuttgart. The wind tunnel is an Eiffel-type wind tunnel with a turbulence levels of $2 \cdot 10^{-4}$. The closed, rectangular test section measures 0.73 m by 2.73 m in cross section and 3.15 m in length. The lift is determined by experimental integration of the pressure distribution alongside the opposite two tunnel walls. The drag is determined, by an integrated wake rake, positioned at approximately 0.45 chord length behind the model's trailing edge. In addition to the polar curves, the pressure distribution of the Mue 13-33 airfoil is measured under stationary conditions. Using the oil-flow-pattern method, a laminar separation bubble at the leading edge becomes visible [11].

In flight test, the Swift S1 and the MDM-1 Fox were equipped with an IMU, GPS and air data sensors. The sensor range is wide enough for all parameters that are of interest for the results. Collected data is mainly used to check comparability of different test flights. To visualize the laminar separation bubble, oil flow patterns are used. Tuft patterns show flow separation on the wing, filmed by a camera that recorded up to 100 frames per second [12].

Results

One type of leading edge stall, distinct from that described in previous literature, is presented below. The characteristic is a laminar separation bubble at the leading edge that is not involved in stall. The flow separates and reattaches in the turbulent boundary layer downstream of the laminar separation bubble at the leading edge.

Development of the Mue 13-33 airfoil

The NACA 64_1-412 airfoil is used for the wing section of the Swift S1 and the MDM-1 Fox. Based only on the knowledge of polar curves and the shape of the airfoil, a new airfoil is designed with the goal of replicating the stall behavior of the NACA airfoil. Basic design requirements are a symmetrical shape and the application of a flap. For comparison, the symmetrical NACA 64_1-012 airfoil was examined, differing from the NACA 64_1-412 only in lack of camber. Polar curves are available [13], but information on hysteresis behavior or pressure distributions at high angles of attack is still missing. A large hysteresis loop and reattachment at small angles of attack can be interpreted as a laminar separation and reattachment during stall. Laminar separation and reattachment can be difficult to handle for the pilot, since the time for flow separation that leads to stall is very short and simultaneously the time for flow reattachment is prolonged in comparison to turbulent flow reattachment. As mentioned above, important information on stall behavior is missing and the precise stall characteristic cannot be explained for the NACA 64_1-412 airfoil. For the low Reynolds numbers of interest here, post stall behavior is not plotted at all, as shown in Fig. 1. The lift characteristics at high angles of attack for a Reynolds number of $3 \cdot 10^6$ show a typical behavior of combined leading and trailing edge stall, including a slight loss of lift coefficient followed by a very high one.Hysteresis behavior that could allow a conclusion about laminar vs. turbulent flow reattachment during reduction of angle of attack after stall is not recorded [13].

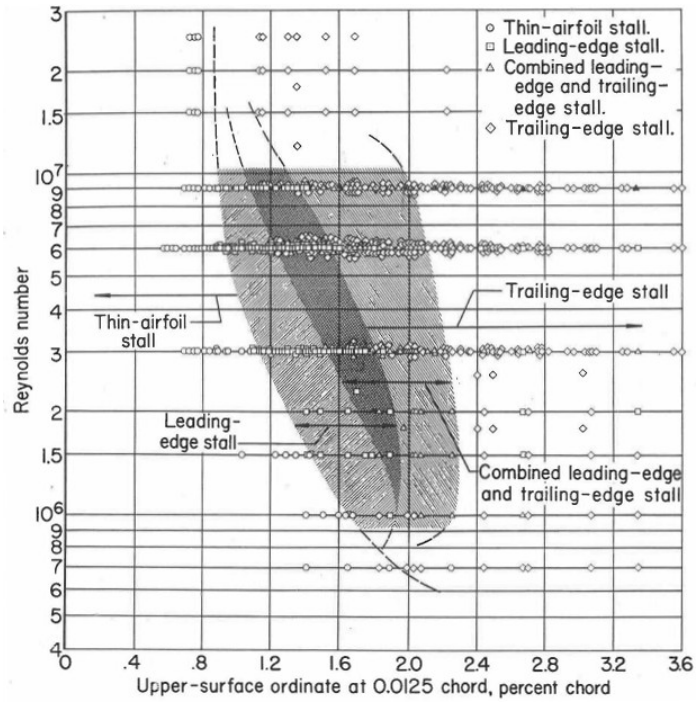

Fig. 2: Chart created by Gault showing stall characteristics dependent on Reynolds Number and nose radius [14].

According to Gault [14], the nose radius is responsible for different stall characteristics, depending on the Reynolds number. The chart in Fig. 2 shows the tendency of a smaller nose radius to provoke leading edge stall. The value of the y-coordinate at 1.25% chord length is a parameter of the resulting nose radius and used by Gault.

Large values of leading edge radius lead to trailing edge stall, while in between combined trailing and leading edge stall can be found. With y/c = 0.0156 at x/c = 0.0125 the nose radius of the Mue 13-33 is chosen to be slightly larger than the nose radius of NACA 64_1-412. Although Gault predicts a leading edge stall and not the desired combined leading and trailing edge stall for relevant Reynolds numbers, the nose radius is chosen similar to the NACA 64_1-412 airfoil (see Fig. 2) [9].

Using the semi-inverse method in XFOIL to optimize the location of transition, depending on an angle of attack suitable for 20% flap or aileron, the symmetric Mue 13-33 airfoil is designed. The results are shown in Fig. 3. The name "Mue 13-33" indicates that the maximum thickness of 13% is positioned at 33% of the chord [9]. The Mue 13-33 airfoil can be compared to the NACA 64_1-412 airfoil shown in Fig. 4.

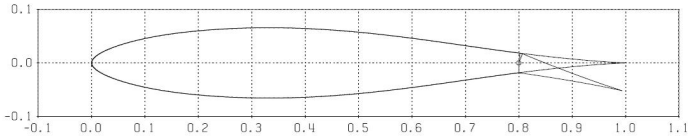

Fig. 3: Mue 13-33 Airfoil geometry [9].

Fig. 4: NACA 64_1-412 airfoil geometry [13].

Flow separation on the Mue 13-33 airfoil under stationary conditions in wind tunnel

In testing the Mue 13-33 airfoil, in addition to the usual lift and drag measurements, special attention is paid to the stall behavior. Pressure distribution and oil-flow-patterns provide information on transition and laminar separation bubbles.

Numerical investigations with ANSYS CFX show a chart for the lift coefficient dependent on angle of attack that is typical for

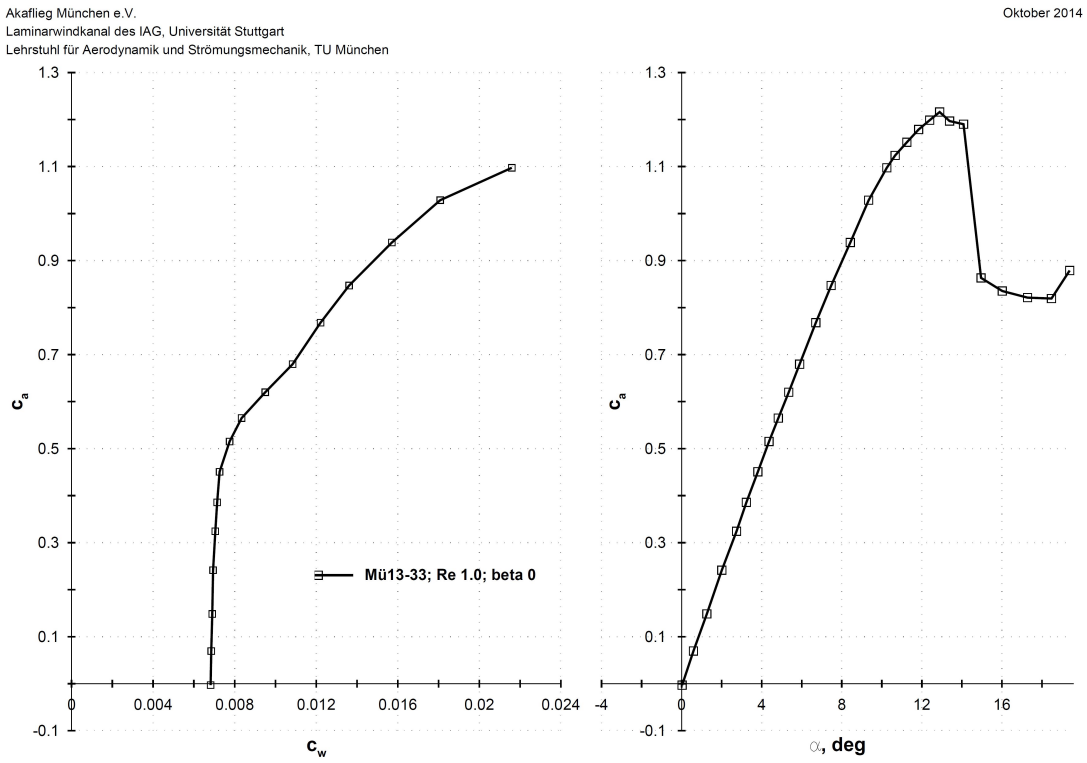

Fig. 5: Drag polar and lift curve at Reynolds number $1 \cdot 10^6$ [11].

combined trailing and leading edge stall, with unusually high lift coefficients. Flow separation is predicted as a trailing edge stall in combination with a growing laminar separation bubble. The bubble bursts at a size of 33% chord length and induces complete stall. There is reasonable doubt due to the fact that the so called "dynamic stall", which can be observed in stationary and dynamic numerical results, is a typical stall behavior of oscillating angles of attack. Since the setup for numerical computation did not include oscillation, dynamic stall should not be predicted [9], [10].

As expected, a different stall behavior can be observed during wind tunnel experiments. A laminar separation bubble is visible in the nonlinear part of the polar curve, showing lift coefficient versus angle of attack. The polar curve in Fig. 5 illustrates the stall behavior as angle of attack varies. At a Reynolds number of $1 \cdot 10^6$, the nonlinear part and the beginning of flow separation at the trailing edge start at 9°. The maximum lift coefficient is measured at 12.9° and the post-stall region begins at about 14.5°. Due to unsteady effects at the moment of complete stall, the angle of attack might vary a little between test runs. However, the characteristics of stall remains the same. At 10° and a Reynolds number of $1 \cdot 10^6$, flow separation at the trailing edge appears at 77% chord length and a laminar separation bubble with a relative size of 0.9% chord length is visible in the oil-flow-pattern, as shown in Fig. 6.

Figure 7 and Fig. 8 show the oil-flow pattern shortly before and after full stall, between 13° and 14° of angle of attack. With increasing angle of attack, the laminar separation bubble maintains its size and moves slightly closer to the leading edge. It is particularly interesting that, even after stall, it remains in its position with no change in size. Turbulent reattachment and a turbulent attached flow are visible downstream of the bubble. The arrows in the schematic sketch in Fig. 8 mark the region of unsteady influence. The question, where the flow separation initiates in the forward part of the airfoil cannot be answered under stationary test conditions [11].

For higher Reynolds numbers, trailing edge stall is less dominant compared to the behavior at $1 \cdot 10^6$. As an example, in Fig. 9 the pressure distributions for Reynolds numbers $1 \cdot 10^6$ and $2.5 \cdot 10^6$ are given for the same angle of attack. Stalled areas are characterized by slightly oscillating, but almost constant pressure distribution at the trailing edge on the upper wing surface. The resulting difference in lift to angle of attack ratio for different Reynolds numbers can be seen in Fig. 10. The loss of lift that occurs at a Reynolds number of $2.5 \cdot 10^6$ is much more rapid compared to polar curves at 0.8 and $1 \cdot 10^6$.

The same figure also shows that hysteresis is present. The hysteresis is not extreme since stall and reattachment are occurring under turbulent flow conditions. In snap rolls and even more so during take-off and landing it is essential to have a reliable reattachment, which implies turbulent reattachment of flow [11].

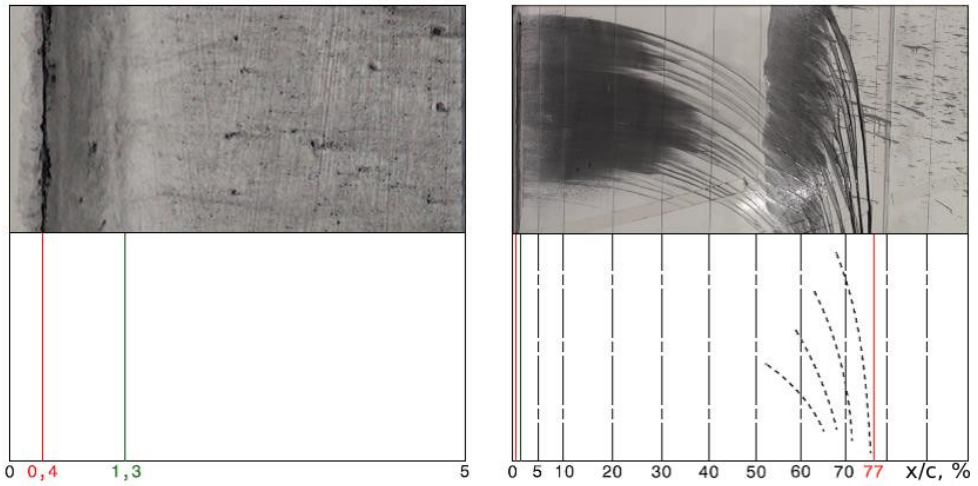

Fig. 6: Laminar separation bubble and flow separation, α = 10°, Re = $1 \cdot 10^6$ (red line: flow separation, green line: reattachment) [11].

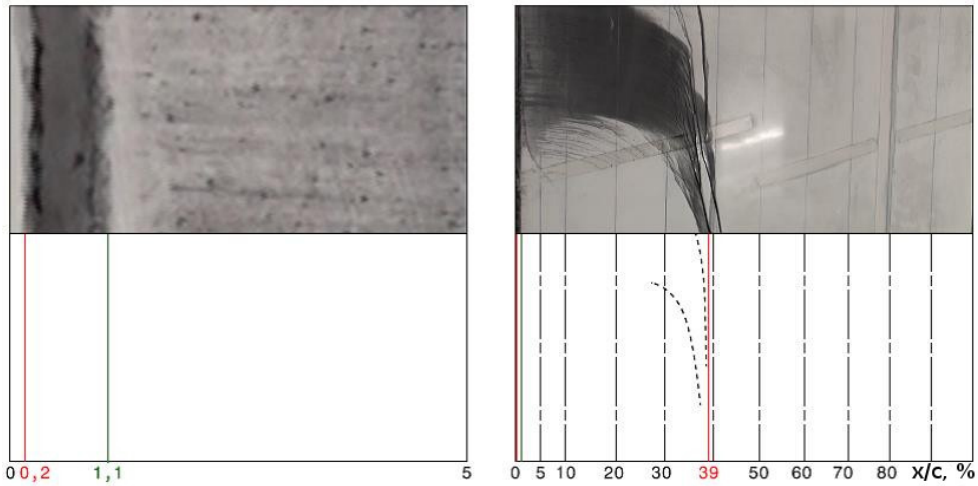

Fig. 7: Laminar separation bubble and flow separation, α= 13°, Re = $1 \cdot 10^6$ [11].

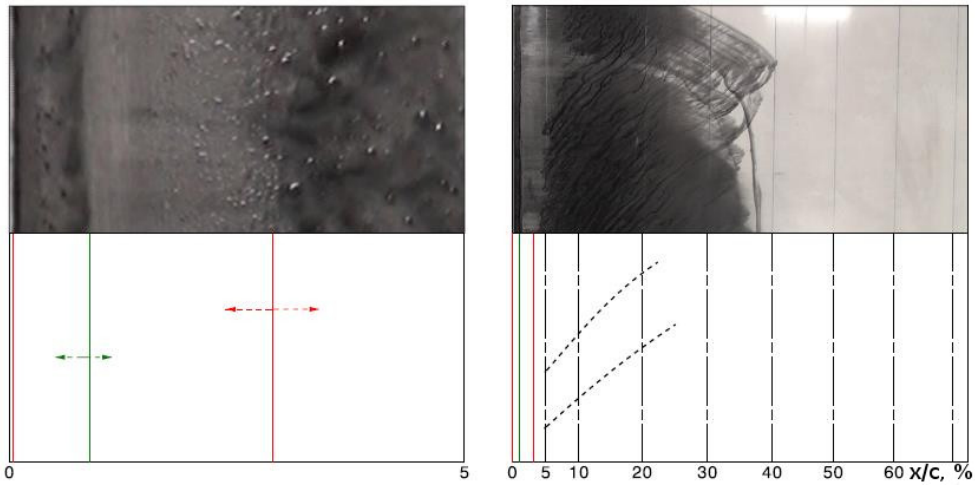

Fig. 8: Laminar separation bubble and flow separation, α= 14°, Re = $1 \cdot 10^6$ [11].

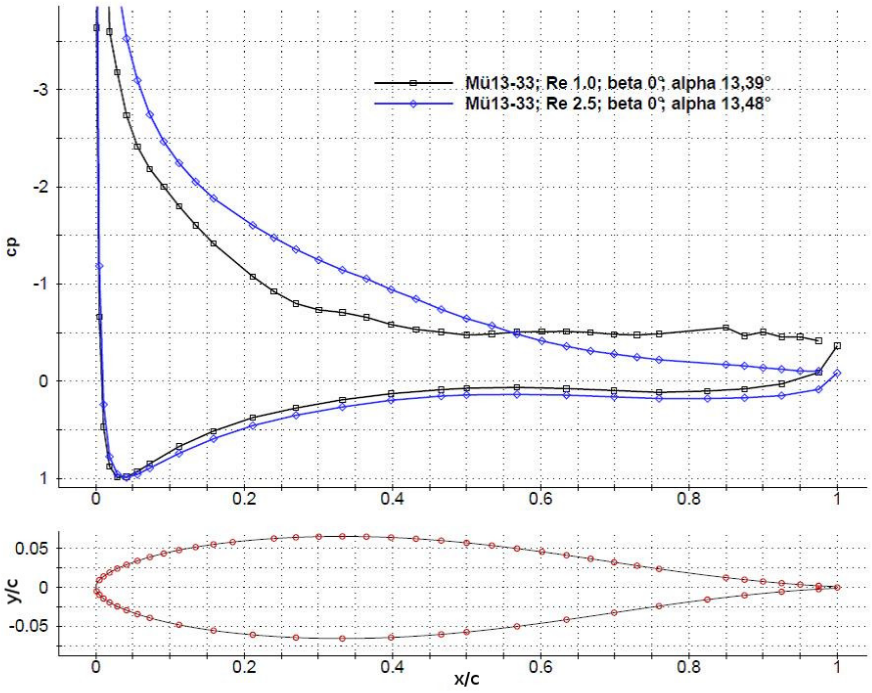

Fig. 9: Pressure distribution for two different Reynolds Numbers [11].

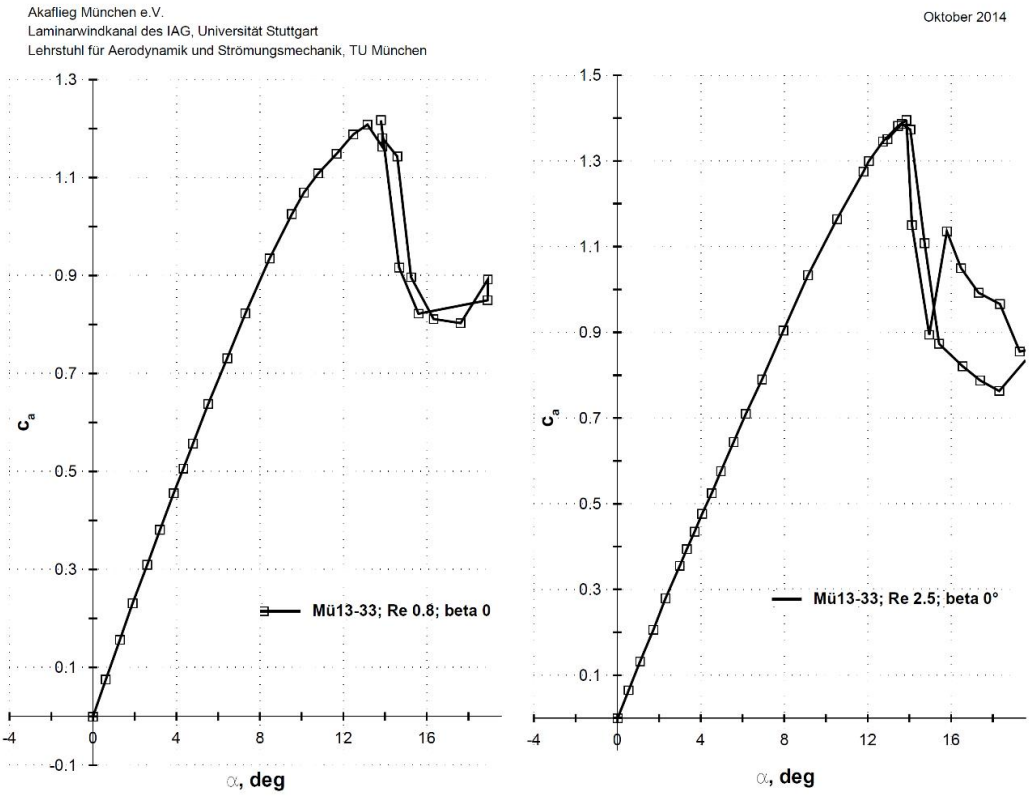

Fig. 10: Lift curves of Mue 13-33 at Reynolds numbers Re = $0.8 \cdot 10^6$ and Re = $2.5 \cdot 10^6$, showing hysteresis [11].

Flight tests with NACA 64_1-412 airfoil to compare flow separation under steady and unsteady conditions

As unsteady wind tunnel tests are difficult to realize and numerical investigations are not sufficient to predict stall behavior, flight tests were carried out both with the Swift S1 and the MDM-1 Fox. Both aerobatic gliders feature the NACA 64_1-412 airfoil. Since the nose radius and polar curves of this airfoil are similar to those of the Mue 13-33 airfoil, it is expected that stall characteristics are similar as well. The flight program includes a quasistationary increase in angle of attack. A vertical acceleration of less than 1g is the criterion for steady flight condition. The results can be compared to wind tunnel measurements. In addition, unsteady angle of attack increases and snap rolls are performed [12].

Comparison of NACA 64_1-412 and Mue 13-33 airfoil under steady conditions

Oil-flow patterns during gradual increase in angle of attack show no different behavior of the bubble at the leading edge. The patterns, however, are less clear than those obtained in the wind tunnel for the Mue 13-33 airfoil. Figures 11 to 13 show a laminar separation bubble at the leading edge of MDM-1 Fox in different conditions around the maximum lift coefficient [12]. The bubble remains at the leading edge in every different flow condition — especially during and after stall. This is the same observation as on the Mue 13-33 airfoil in wind tunnel tests, as shown previously in Figs. 6 to 8 [11].

Surface tufts on NACA 64_1-412 under steady and unsteady conditions

The tuft patterns on the wing provide the location of separated flow areas. In comparison to the oil-flow technique, the tuft pattern method is well suited for experiments under dynamic and unsteady movements. However, the location of boundary layer transition cannot be determined, and instead the tufts trigger the transition. With the stall beginning at the trailing edge, the flow is fully turbulent downstream of the laminar separation bubble at the leading edge. Therefore, no influence of tufts on the stall behavior is expected. Figures 14–15 illustrate the progression of the stall along the wing based on the tuft observations. Attached tufts are black and separated ones grey. In the figures, time stamps are provided to aid the comparison of the stall behavior. However, the times shown are not synchronized with the measured data. Three-dimensional effects that lead to the observed patterns cannot be excluded [12].

The MDM-1 Fox wing is more highly tapered than that of the Swift S1. Therefore, the spanwise development of the stall is more pronounced in the MDM-1 Fox. Figure 14 shows tuft patterns for the steady increase in angle of attack at the wing section of the MDM-1 Fox. Sectionwise flow separation starts at the trailing edge and ends in a sudden flow separation between

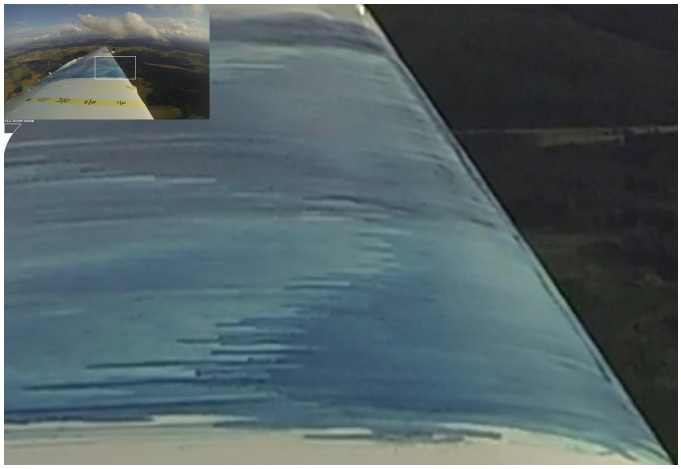

Fig. 12: Oil flow pattern on wing of MDM-1 Fox in stall [12].

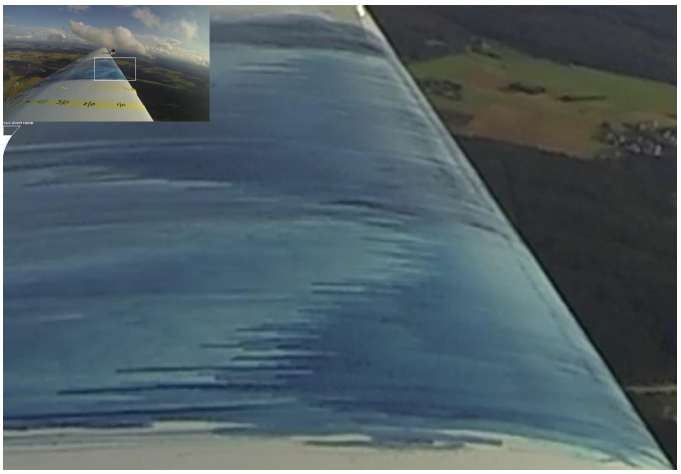

Fig. 11: Oil flow pattern on wing of MDM-1 Fox at high angle of attack [12].

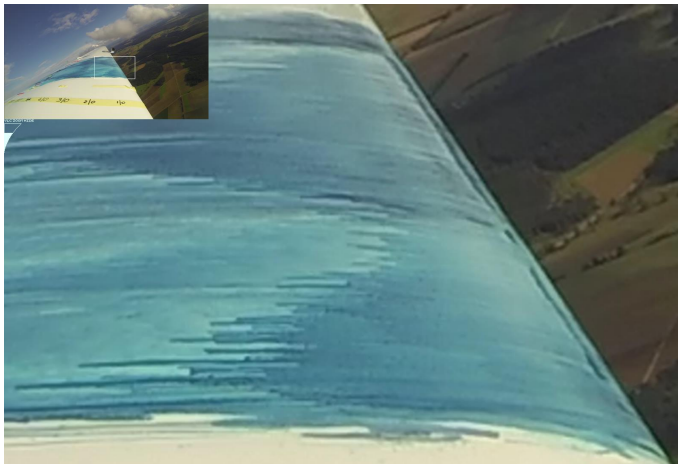

Fig. 13: Oil flow pattern on wing of MDM-1 Fox during reattachment [12].

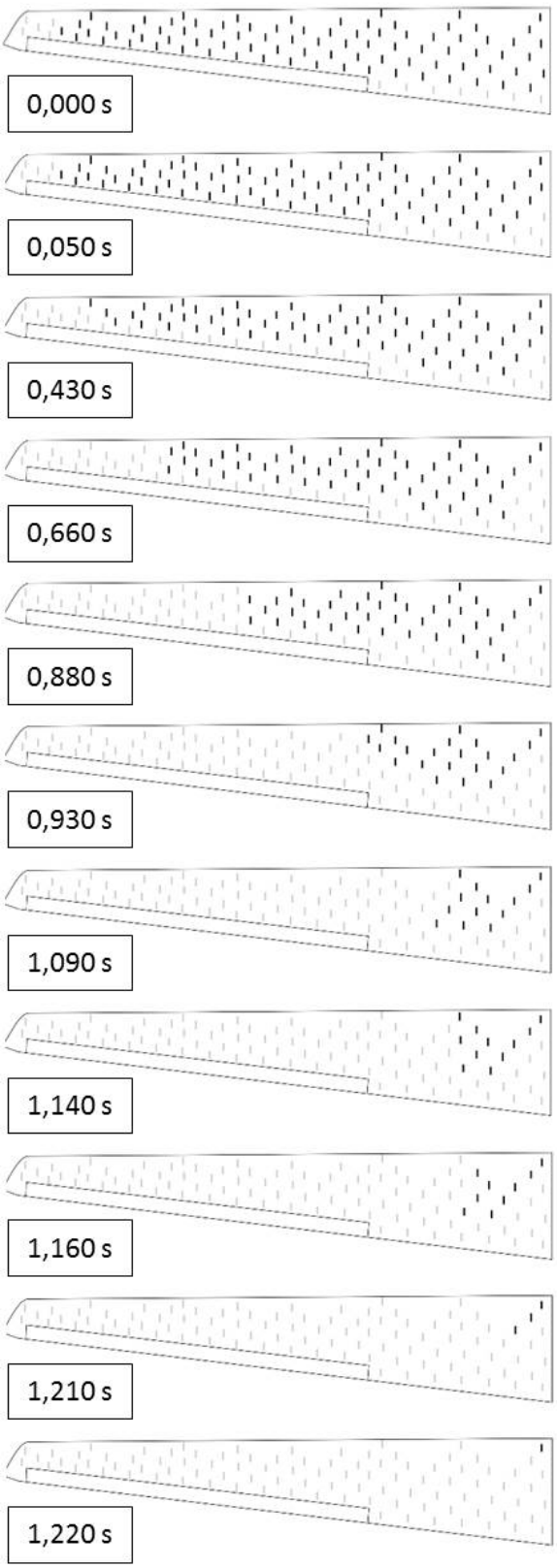

Fig. 14: Tuft pattern during steady increase of angle of attack on wing of MDM-1 Fox [12].

the leading edge and the position of maximum thickness of the airfoil section. Dynamic increase in angle of attack (more than $10^\circ/\mathrm{s}$) gives more detailed information on what might happen at the leading edge during stall, since the increase in angle of attack is much smoother. The stall process in the tuft patterns of Fig. 15 shows the beginning of flow separation at the trailing edge, for the Swift S1 as well as for the MDM-1 Fox. In case of the MDM-1 Fox, this is a very systematic angular pattern. The stalled area progresses from the outer wing towards the fuselage, starting always at the leading edge. For the Swifts wing section, a less orderly flow separation at the leading edge can be observed. Nevertheless, parts of attached flow close to the maximum thickness of the airfoil, and at the same time stalled parts at the leading edge, are visible [12].

Observations of tuft patterns during snap rolls, including variations in use of ailerons, do not reveal different characteristics of stall, unlike simple steady and dynamic increase in angle of attack. Due to the yaw motion and a greater decrease in Reynolds number in the outer part of the wing, this region stalls earlier than the area close to the aircrafts body. Experiments on the aerobatic glider Mü 28, with negative flap deflection in order to induce snap rolls, show an earlier stall compared to neutral flap deflection close to the body, where the flaps are positioned. The pressure distribution is modified in a way that provokes stall at higher Reynolds numbers and lower angles of attack, compared to a plain airfoil [12].

As a result, no difference in stall characteristics between steady and unsteady conditions can be observed. Flow separation at the front section of the airfoil, between the leading edge and the point of maximum airfoil thickness, is turbulent under all tested conditions, as the constant presence of the laminar separation bubble confirms [12].

Conclusions

Combined leading and trailing edge stall, with turbulent flow separation at the leading edge, can be observed on the Mue 13-33 and the NACA 64_1-412 airfoils. Flight tests with the NACA 64_1-412 airfoil show the suitability of this airfoil's stall type for dynamic stall and especially snap rolls in aerobatic flight. Trailing edge stall ensures good flying qualities at low airspeeds and high lift coefficients. Turbulent flow separation and reattachment at the leading edge prevent critical hysteresis effects. The concept of the Mü 32 Reißmeister includes flaps that support quick flow separation close to the body during snap rolls.

References

[1] Schlichting, H. and Truckenbrodt, E., *Aerodynamik des Flugzeuges, Band I*, Springer-Verlag, Berlin Göttingen Heidelberg, 1960.

[2] Marxen, O., "Laminar-Turbulent Transition in a Laminar Separation Bubble: Influence of Disturbance Amplitude on Bubble Size and Bursting." *High Performance Computing in Science and Engineering '07*, edited by W. E. Nagel, D. Kröner, and M. Resch, Springer-Verlag, Berlin Heidelberg, 2008, pp. 261–275.

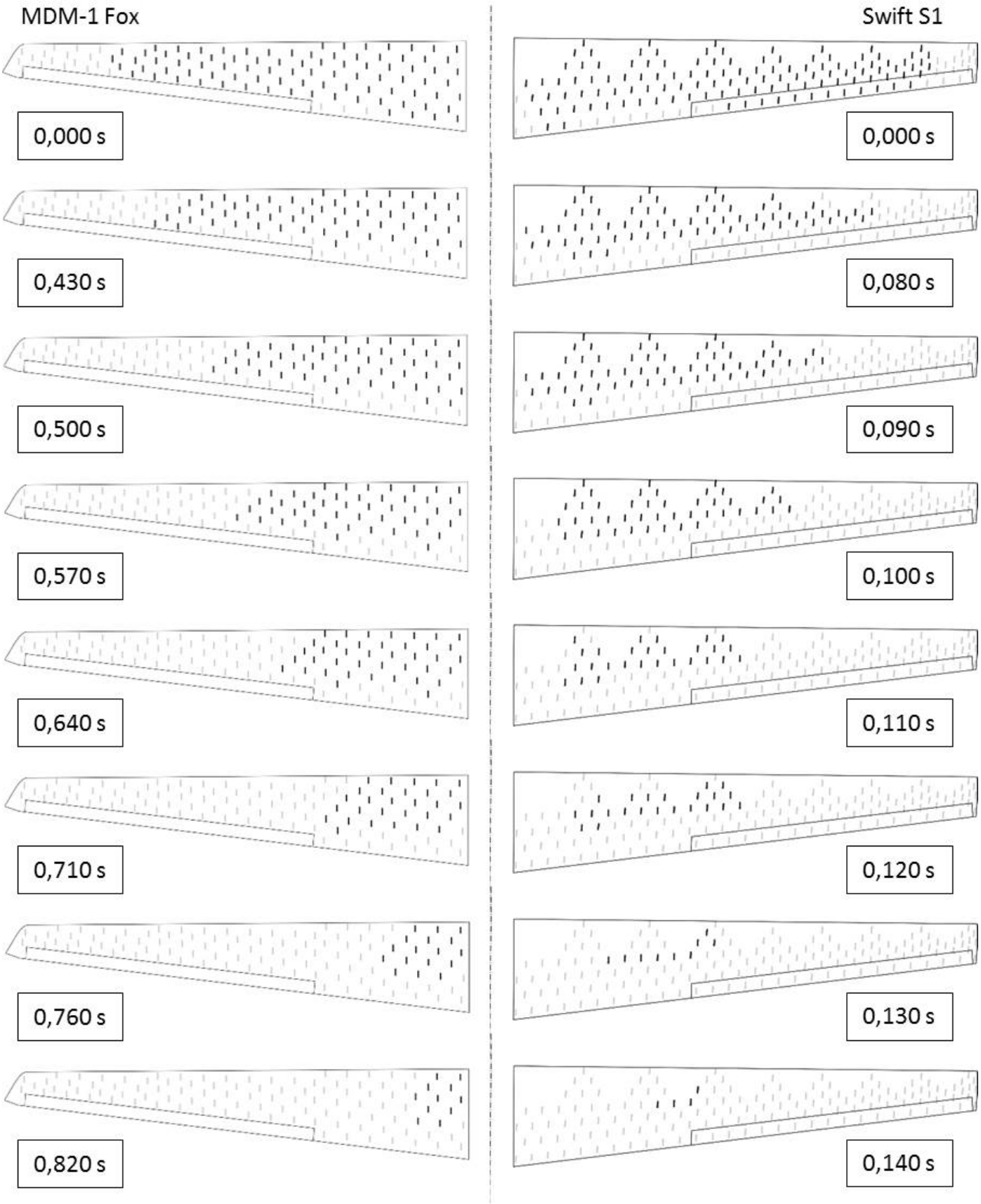

Fig. 15: Dynamic increase of angle of attack on wing of Swift S1 and MDM-1 Fox [12].

[3] Gaster, M., "The structure and behaviour of laminar separation bubbles." *AGARD CP-4*, 1966, pp. 813–854.

[4] Lang, M., Rist, U., and Wagner, S., "Investigations on controlled transition development in a laminar separation bubble by means of LDA and PIV." *Experiments in Fluids*, Vol. 36, No. 1, 2004, pp. 43–52.

[5] Rist, U., *Zur Instabilität und Transition in laminaren Ablöseblasen*, Habilitationsschrift, Universität Stuttgart, 1998, Shaker Verlag, Aachen.

[6] Diwan, S. S., Chetan, S. J., and Ramesh, O. N., "On The Bursting Criterion For Laminar Separation Bubbles." *IUTAM Symposium on Laminar-Turbulent Transition*, edited by R. Govindarajan, Vol. 78 of *Fluid Mechanics and Its Applications*, Springer, Dordrecht, 2006, pp. 401–407.

[7] Greenblatt, D. and Wygnanski, I. J., "Effect of Leading-Edge Curvature on Airfoil Separation Control." *Journal of Aircraft*, Vol. 40, No. 3, 2003, pp. 473–481.

[8] Ranke, H., *Instationäre Grenzschichtablösung in ebener, inkompressibler Strömung*, Dissertation, Technische Universität München, 1998.

[9] Sturm, F., *Entwurf eines Tragflügelprofils für Segelkunstflug und Untersuchung der Abrisseigenschaften mit ANSYS CFX*, Semester thesis, Institute of Aerodynamics and Fluid Mechanics, Technische Universität München, 2013.

[10] Pattermann, R., *Untersuchungen der Ablösecharakteristik eines Tragflügels für ein Segelkunstflugzeug mittels numerischer Strömungssimulation*, Semester thesis, Institute of Aerodynamics and Fluid Mechanics, Technische Universität München, 2014.

[11] Döller, B., *Windkanaluntersuchungen zum Profilentwurf für ein Segelkunstflugzeug*, Semester thesis, Institute of Aerodynamics and Fluid Mechanics, Technische Universität München, 2014.

[12] Pattermann, R., *Auswertung von Flugversuchen zur Untersuchung des Abreißverhaltens von Segelkunstflugzeugen im Hinblick auf die aerodynamische Auslegung der Mü 32*, Semester thesis, Institute of Aerodynamics and Fluid Mechanics, Technische Universität München, 2015.

[13] Loftin, L. K. J. and Smith, H. A., "Aerodynamic characteristics of 15 NACA airfoil sections at seven Reynolds Numbers from $0.7 \cdot 10^6$ to $9.0 \cdot 10^6$." Technical Note TN-1945, NACA, 1949.

[14] Gault, D. E., "A correlation of low-speed, airfoil-section stalling characteristics with Reynolds Number and airfoil geometry." Technical Note TN-3963, NACA, 1957.